Huang et al. Nanoscale Research Letters (2017) 12:541
DOI 10.1186/s11671-017-2308-1

Nanoscale Research Letters

NANO EXPRESS Open Access

Fermi Level Tuning of ZnO Films Through Supercycled Atomic Layer Deposition

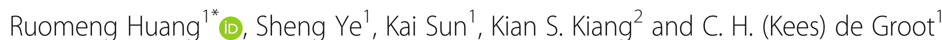
Ruomeng Huang[1*], Sheng Ye[1], Kai Sun[1], Kian S. Kiang[2] and C. H. (Kees) de Groot[1]

Abstract

A novel supercycled atomic layer deposition (ALD) process which combines thermal ALD process with in situ O_2 plasma treatment is presented in this work to deposit ZnO thin films with highly tunable electrical properties. Both O_2 plasma time and the number of thermal ALD cycles in a supercycle can be adjusted to achieve fine tuning of film resistivity and carrier concentration up to six orders of magnitude without extrinsic doping. The concentration of hydrogen defects are believed to play a major role in adjusting the electrical properties of ZnO films. Kelvin probe force microscopy results evidently show the shift of Fermi level in different ZnO films and are well associated with the changing of carrier concentration. This reliable and robust technique reported here clearly points towards the capability of using this method to produce ZnO films with controlled properties in different applications.

Keywords: Fermi level, ZnO, Atomic layer deposition, Kelvin probe force microscopy

Background

Once defined as the *future material*, zinc oxide (ZnO) has attracted the interest of science community for over half a century due to its superior optical and electrical properties [1]. Recently, the rapid growth of transparent conductive oxide industry has further revived its application as transparent electrodes in flat panel displays, touch screens, low emissivity coating, thin film solar cells, etc. [2, 3]. Furthermore, ZnO has found numerous applications in electronic devices including light-emitting diodes, photo detectors, and power devices [4, 5]. These different types of applications require ZnO films to have various electrical parameters, and some applications even demand multi-layer of ZnO films with different electrical properties [6]. For example, numerous efforts have been made to develop transparent resistive random access memory (TRRAM) for the realization of fully integrated transparent electronics [7, 8]. As one of the most promising candidates, ZnO-based TRRAM uses a highly resistive ZnO film as the active switching layer while highly conductive ZnO films are ideally demanded to act as transparent electrodes [8–10]. The capability of controlling the electrical properties such as resistivity and carrier concentration of the ZnO films is therefore a key requirement. Doping is usually used when the property modification is needed and a variety of dopants have been applied to change ZnO film properties [11–13]. However, doping is always complex and could lead to the secondary phase formation [14]. Modulation of the electrical properties of undoped ZnO by a single deposition process can therefore be advantageous.

Atomic layer deposition (ALD) has become a popular technique to form high-quality ZnO with an excellent control of the film thickness down to nanometer scale and uniformity over a large substrate [15, 16]. The growth temperature of ZnO is usually under 200 °C which makes it compatible with a range of substrates including glass and plastics. The ALD ZnO is normally grown by using diethylzinc (DEZ) as a Zn precursor and water vapor (thermal) or oxygen plasma (plasma-enhanced) as oxygen precursor. The dominant way of tuning undoped ZnO film properties in the thermal ALD process is by changing the growth temperature [17, 18]. Although this enables the deposition of highly conductive films, high-quality ZnO films are difficult to obtain with low carrier concentration. The plasma-enhanced ALD is preferably used when low-carrier concentration ZnO is required [19, 20]. We recently reported the capability of tuning ZnO using a single plasma-enhanced ALD process which allows the tuning of its resistivity

* Correspondence: r.huang@soton.ac.uk
[1]Nanoelectronics and Nanotechnology Group, Department of Electronics and Computer Science, University of Southampton, Southampton SO17 1BJ, UK
Full list of author information is available at the end of the article

Springer Open

© The Author(s). 2017 **Open Access** This article is distributed under the terms of the Creative Commons Attribution 4.0 International License (http://creativecommons.org/licenses/by/4.0/), which permits unrestricted use, distribution, and reproduction in any medium, provided you give appropriate credit to the original author(s) and the source, provide a link to the Creative Commons license, and indicate if changes were made.

and carrier concentration up to three orders by using different O_2 plasma times [21]. However, the plasma-enhanced ALD could suffer a non-self-limiting growth if a short O_2 plasma time is applied to achieve needed carrier concentration, which can result in poor uniformity over a large substrate. A tunable ALD process within the self-limiting window would therefore be desired.

Apart from the capability in tuning the ZnO electrical properties, determination of these properties also remains challenging. Hall effect measurement is the most popular technique in measuring the electrical properties of ZnO thin films. However, it can be prone to misinterpretation and has difficulty in unambiguous detection of the actual cause of doping [1]. Kelvin probe force microscopy (KPFM) is a non-destructive surface technique which has been extensively used to characterize nanoscale structural, dynamic, and electrical properties of semiconductor materials and devices [22, 23]. By directly measuring the contact potential difference (V_{CPD}), i.e., the difference between the work functions of the tip and the sample, it can provide an insight into the material dopant types, carrier concentrations, and resistivity as they affect the Fermi level position within the bandgap. However, works correlating the ZnO properties with KPFM results are rarely reported, and to our knowledge, there are none based on ALD-grown ZnO films [24–26].

In this work, we propose a novel supercycled ALD process for electrical properties tuning in undoped ZnO. Combining the thermal ALD process with an in situ O_2 plasma treatment, this process allows a wide yet refined tuning of the ZnO film resistivity and carrier concentration. More importantly, the Fermi level shifts in the ZnO films can be directly measured by KPFM and used to characterize the ZnO electrical properties.

Methods

All ZnO thin films were prepared in an OIPT FlexAl ALD system using a diethylzinc (DEZ) precursor. Each supercycle of the ALD process consists of *m* cycles of thermal ALD processes (DEZ and H_2O) and one O_2 plasma step as demonstrated in Fig. 1a. Within the thermal ALD process, DEZ vapor was initially introduced into the chamber and then purged by an argon flow, and H_2O vapor was subsequently introduced and then argon purged. After *m* cycles of thermal ALD processes, an O_2 plasma step was added as an in situ plasma treatment step. The O_2 plasma step was set using an O_2 flow of 60 sccm, RF power of 300 W, and pressure of 15 mTorr. Both thermal ALD numbers (*m*) and O_2 plasma time (t_3) were used for ZnO film property control. The specific details for one growth supercycle in the ALD process are given in Additional file 1: Table S1. All ZnO films were deposited on the SiO_2-coated Si substrates (1 cm × 1 cm) at a fixed temperature of 190 °C, and all film thicknesses were projected to be 40 nm.

The thickness and optical constants of the deposited ZnO films were measured by ellipsometry (VASE, J.A. Woollam Co. M-2000) and fitted with a Tauc-Lorentz (TL) model. The electrical properties were measured by Hall measurements (Nanometrics HL5500PC) at room temperature under a magnetic field of 0.5 T. Extra care was taken to ensure linear contact was obtained between each copper probe and the sample before every single measurement. X-ray diffraction (XRD) patterns were collected in grazing incidence (θ_1 = 1°) using a Rigaku Smartlab diffractometer with a 9-kW Cu-K_α source. X-ray photoelectron spectroscopy (XPS) data were obtained using a Thermo Scientific Theta Probe System with Al-K_α radiation (photon energy = 1486.6 eV). Where necessary, surface contamination was eliminated by the use of an ion sputtering gun. The Zn 2*p*, O 1*s*, and C 1*s* spectra were collected. All data were referenced to the C 1*s* peak, which was assigned a binding energy of 284.6 eV. KPFM measurements were performed on Nanonics CV2000 by a Nanosensor ATEC Pt-Ir-coated tip with a resonant frequency of 65 kHz. To reduce the influence of surface contaminant, the measurements were carried out just after the samples were removed from the vacuum chamber.

Results and Discussion

The proposed supercycled ALD process is illustrated in Fig. 1a with one supercycle consisting of *m* cycles of thermal ALD processes (DEZ and H_2O) and one O_2 plasma step (O_2 plasma). More details are in the "Methods" section. Figure 1b compares the ZnO growth rates in our supercycled ALD process when *m* = 1 and the conventional plasma-enhanced ALD process as a function of O_2 plasma time. The growth rate in the plasma-enhanced ALD process (red) is found to be sensitive to the O_2 plasma as it increases from ca. 1.4 to 1.7 Å/cycle with the plasma time changing from 2 to 4 s. It is then saturated at the level of ca. 1.7 Å/cycle at longer plasma times. The unsaturated growth rate at shorter O_2 plasma time is attributed to the oxygen deficiency in the process. Although this is sometimes preferred to obtain ZnO films with high conductivity, it is not self-limiting and could result in a poor uniformity over the whole substrate. On the other hand, the growth rate was found to be stable at ca. 1.69 Å/supercycle in the supercycled ALD process (black) and is close to that of the thermal ALD process (t_3 = 0 s) regardless of the plasma time applied. Moreover, increase of the thermal cycle *m* in one supercycle with fixed plasma time leads to a linear increase of the growth rate as shown in Fig. 1c. The fitted gradient is calculated to be 1.67 for both growths with different O_2 plasma times, which is also close to the growth rate of the thermal ALD

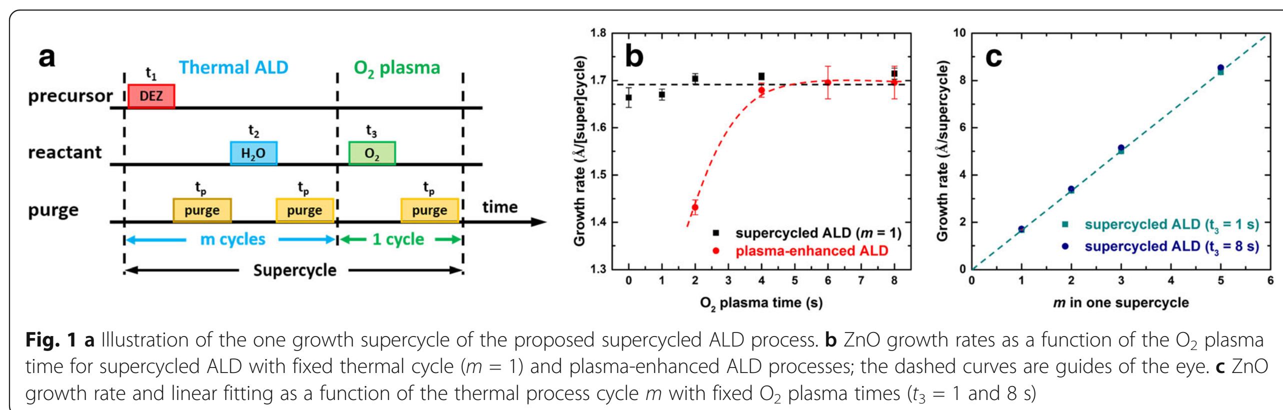

Fig. 1 **a** Illustration of the one growth supercycle of the proposed supercycled ALD process. **b** ZnO growth rates as a function of the O_2 plasma time for supercycled ALD with fixed thermal cycle (m = 1) and plasma-enhanced ALD processes; the dashed curves are guides of the eye. **c** ZnO growth rate and linear fitting as a function of the thermal process cycle m with fixed O_2 plasma times (t_3 = 1 and 8 s)

process. This suggests the growth of ZnO in our supercycled ALD is dominated by the thermal ALD process and the subsequent O_2 plasma step serves as merely a treatment.

All ZnO films grown by the supercycled ALD process (m = 1) crystallize in the hexagonal wurtzite structure and illustrate a similar distribution of peak intensities regardless of the O_2 plasma time, as shown in Fig. 2a. Compared with the theoretical intensity ratio of 0.44 between peak (0 0 2) and (1 0 1) (calculated from JCPDS-34-1451 for a random orientation of the crystallites), these films demonstrate a strong preferred orientation along the c-axis with the (0 0 2) and (1 0 1) peak intensity ratio between 2 and 5, suggesting good crystalline quality of the films. A slight increase of the (0 0 2) to (1 0 1) peak ratio is observed with increasing O_2 plasma time (shown in the Additional file 1: Figure S1). This suggests a higher degree of preferred orientation when exposed to longer plasma. Similar behavior was also reported [27, 28]. However, it is worth pointing out that the change of the intensity ratio in our work is rather trivial compared with others. This further suggests the stability of our supercycled ALD process for producing high quality ZnO films. The average grain sizes was also estimated based on the Scherrer formula [29] and were found to be ca. 11 nm, suggesting the ZnO grain size was barely affected by the O_2 plasma time. Similar patterns are also observed on ZnO films grown from various thermal ALD cycles (m) with a fixed O_2 plasma time (1 s) as shown in Fig. 2b.

Aside from the crystallinity, the optical properties of the supercycled ALD-grown ZnO films were also studied using spectroscopic ellipsometry (SE). Optical constants (n and k) can be extracted from the ellipsometry results by a Tauc-Lorentz model which is commonly used in fitting ZnO films [28, 30, 31]. Similar to the analogous crystallinity, the optical properties of ZnO films deposited with different O_2 plasma times and thermal cycles also remain unchanged as shown in Additional file 1: Figure S2. This is consistent with the reported works that a change of crystallinity is always associated with a change of optical properties [28, 32]. The morphological properties of the ZnO films are characterized by AFM. All films were found to be similarly smooth with average roughness between ca. 0.3 and 0.8 nm (Additional file 1: Figure S3).

The electrical properties of the ZnO films grown by the supercycled ALD process are investigated by a Hall effect system. All films were found to be n-type semiconducting,

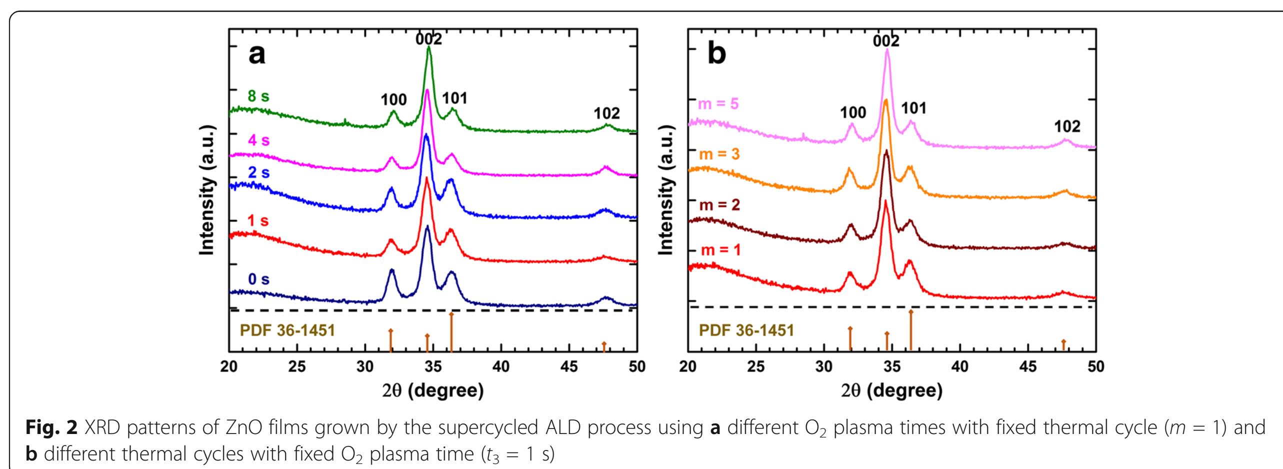

Fig. 2 XRD patterns of ZnO films grown by the supercycled ALD process using **a** different O_2 plasma times with fixed thermal cycle (m = 1) and **b** different thermal cycles with fixed O_2 plasma time (t_3 = 1 s)

and the resistivity increases from ca. 10^{-3} to 10^{3} Ω cm with increasing O_2 plasma time and fixed thermal cycle (m = 1) as shown in Fig. 3a. This is associated with the reduction of the carrier concentration from ca. 10^{21} to 10^{15} cm^{-3} as the O_2 plasma time increases from 0 to 8 s (Fig. 3b). In contrary, the electron mobilities of all ZnO films are found to be rather consistent (ca. 3.0 ± 1.0 cm^2/V s) and are not affected by the plasma duration. The detailed conducting mechanism will be addressed further in the section below. Compared with the plasma-enhanced ALD process we reported earlier [21], the magnitude of resistivity tuning has been further improved in the supercycled ALD process to over five orders. In addition, this proposed ALD process offers a more refined control over these electrical properties by varying the thermal cycle (m) in one supercycle while fixing the O_2 plasma time (t_3). This is particularly useful in the case of t_3 = 1 s where tuning is not achievable by further reducing the plasma time due to the limitation of the ALD equipment. The open dots in Fig. 3a, b represent the resistivities and carrier concentrations of ZnO films grown by different thermal cycles (m = 2, 3, 5) when t_3 = 1 s (error bars are within the dots). It can be observed that more thermal cycles result in less resistive films with higher carrier concentrations. This provides an extra of three resistivities within the range of 10^{-3} to 10^{1} Ω cm.

KPFM measurements were performed to gain insights into the Fermi level positions of the ZnO films with changing resistivity. It measures the contact potential difference V_{CPD} between a conductive tip and the sample which is defined as:

$$V_{CPD} = \frac{\phi_{tip} - \phi_{sample}}{q} \quad (1)$$

where q is the electronic charge, while ϕ_{tip} and ϕ_{sample} are the work function of the tip and the sample respectively. When two different materials are brought into electric contact, the Fermi levels will line up through electron current flow which consequently induces a contact potential difference between the tip and sample as shown in Additional file 1: Figure S4. Detailed working principle of KPFM is presented in Additional file 1. The contact potential differences of the ZnO films grown by the supercycled ALD process from different O_2 plasma times with fixed thermal cycle (m = 1) are shown in Fig. 4. While each V_{CPD} image appears to be uniform and relatively smooth, substantial differences in the mean V_{CPD} values can be observed (shown in Fig. 4f). The tip work function ϕ_{tip} remains constant for all measurements; the substantial difference in V_{CPD} is therefore the consequence of the Fermi level shift within different ZnO films. A total shift of ca. 0.32 eV is obtained between ZnO film grown with 0 and 8 s O_2 plasma time which is significant compared to the ZnO bandgap (ca. 3.22 eV based on the SE results in this work as shown in Additional file 1: Figure S2c). For ZnO films grown from different thermal cycles (m = 2, 3, 5) at fixed O_2 plasma time (t_3 = 1 s), different V_{CPD} values were also detected as shown in Fig. 4f. The two-dimensional KPFM images of these films can be found in Additional file 1: Figure S5. This implies the change in the electron-hole balance occurs throughout the films which could make considerable impact to the ZnO carrier concentration.

In order to investigate the relation between the Fermi level and carrier concentration, we adopt the electronic energy model proposed by Maragliano et al. to correlate the contact potential difference V_{CPD} with the doping concentration in the material [26]. Assuming the effective donor concentration n_D is significantly higher than the intrinsic carrier concentration, it can be written as:

$$n_D \approx N_C \exp\left(\frac{qV_{CPD} - \phi_{tip} + \chi}{K_B T}\right) \quad (2)$$

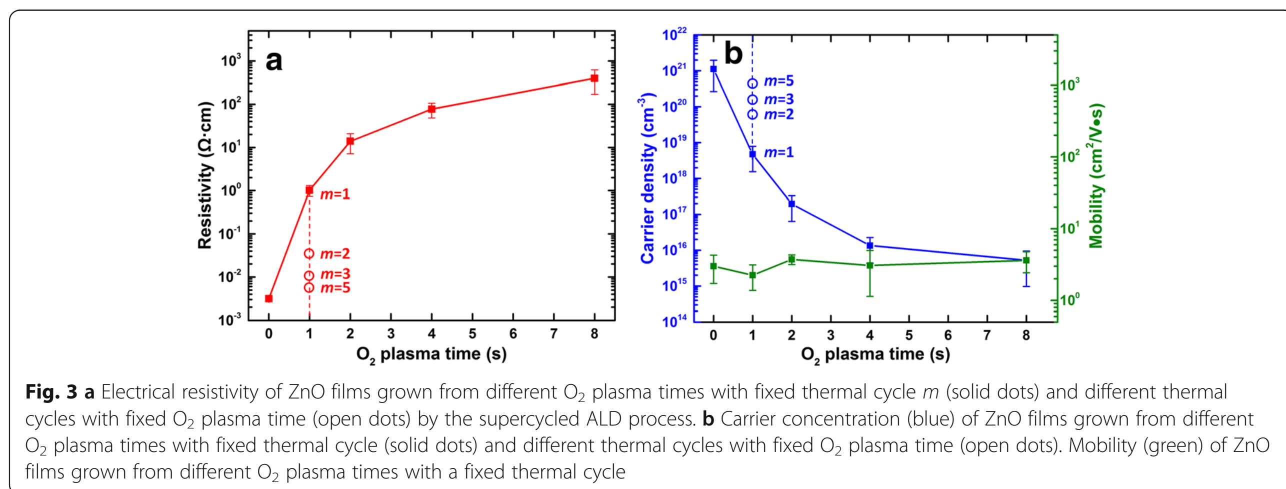

Fig. 3 a Electrical resistivity of ZnO films grown from different O_2 plasma times with fixed thermal cycle m (solid dots) and different thermal cycles with fixed O_2 plasma time (open dots) by the supercycled ALD process. **b** Carrier concentration (blue) of ZnO films grown from different O_2 plasma times with fixed thermal cycle (solid dots) and different thermal cycles with fixed O_2 plasma time (open dots). Mobility (green) of ZnO films grown from different O_2 plasma times with a fixed thermal cycle

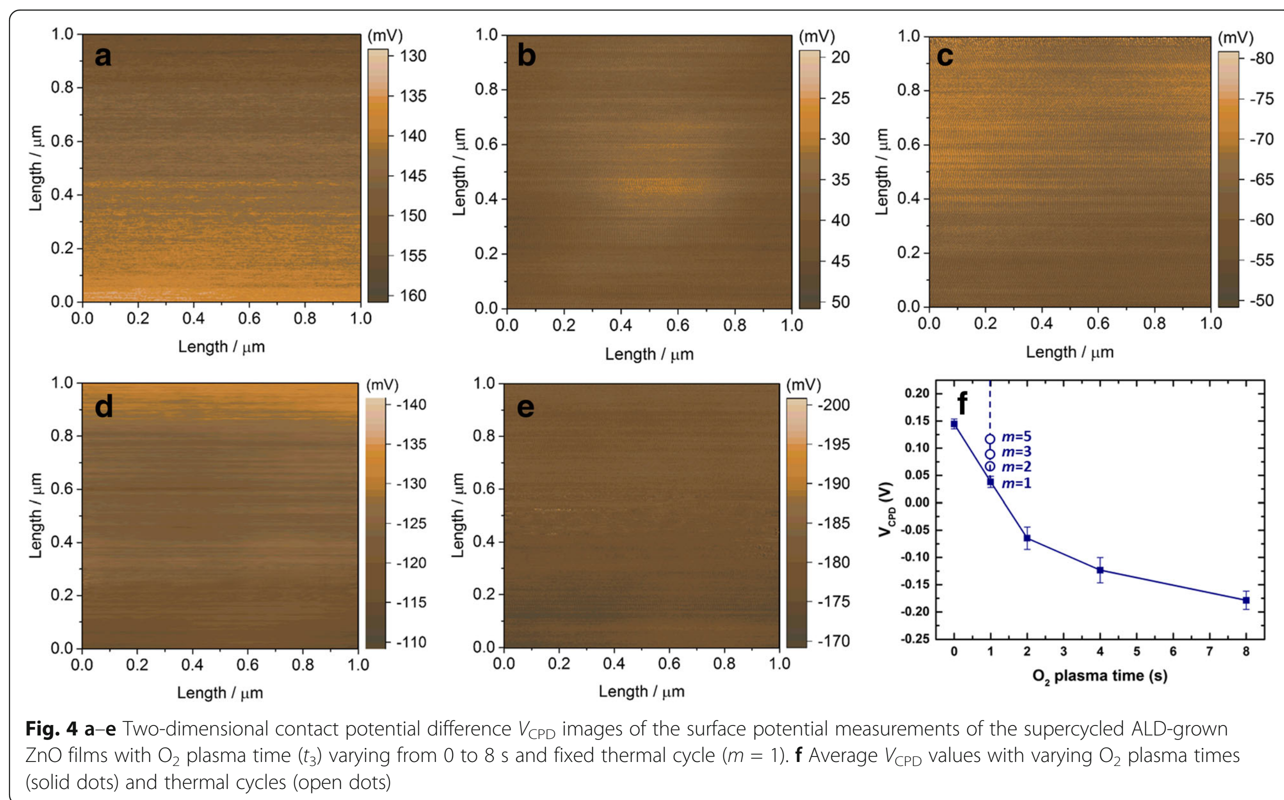

Fig. 4 a–e Two-dimensional contact potential difference V_{CPD} images of the surface potential measurements of the supercycled ALD-grown ZnO films with O_2 plasma time (t_3) varying from 0 to 8 s and fixed thermal cycle (m = 1). **f** Average V_{CPD} values with varying O_2 plasma times (solid dots) and thermal cycles (open dots)

where N_C is the effective density of states, χ is the electron affinity of the semiconductor, K_B is the Boltzmann constant, and T is the temperature. Although the values of the effective density of states N_C, the tip work function ϕ_{tip}, and the electron affinity χ are difficult to obtain, the relative carrier concentration differences of different ZnO films can be calculated as these values are the same in all measurements. Hence, the carrier concentration ratio between the films grown with 0 s of O_2 plasma time to a given ZnO film can be expressed as:

$$\frac{n_0}{n_x} = \exp\left(\frac{V_{CPD0}-V_{CPDx}}{K_B T/q}\right) \tag{3}$$

in which n_0 and n_x are the carrier concentration of the ZnO film grown with 0 and x s of O_2 plasma time, respectively, and V_{CPD0} and V_{CPDx} are the corresponding contact potential differences. The calculated carrier concentration ratios are plotted in Fig. 5 as a function of O_2 plasma time. The concentration ratio is calculated to increase with longer O_2 plasma time (red). More importantly, the increasing trend matches well with the values obtained from the Hall effect measurement results (black). Similar trend was also observed for ZnO films grown from different thermal cycles (m = 2, 3, 5) at fixed O_2 plasma time (t_3 = 1 s). This evidently suggests the shift of ZnO film Fermi level is directly associated with the carrier concentration level.

X-ray photoelectron spectroscopy (XPS) measurements were carried out to shed light on the conduction mechanism by studying the bonding and chemical states of the supercycled ALD-grown ZnO films. The chemical states of O 1s are shown in Fig. 6 where two peaks can be identified after Gaussian fittings. The lower energy peak (A) positioned ca. 530.3 eV is suggested to be the O^{2-} ions in the wurtzite structure of hexagonal Zn^{2+}

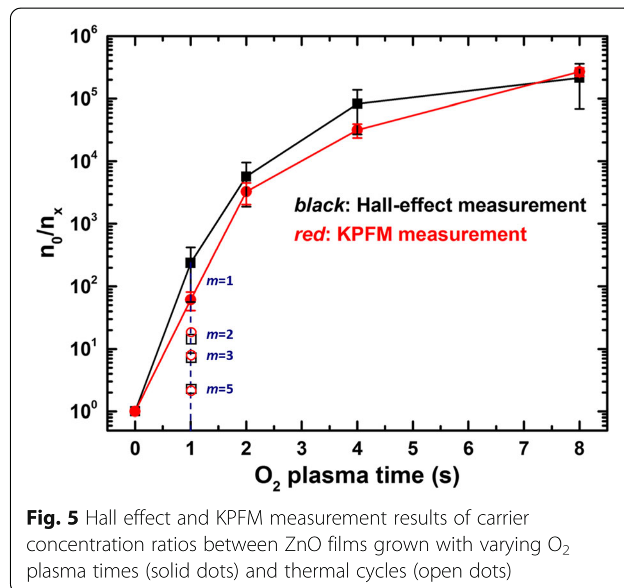

Fig. 5 Hall effect and KPFM measurement results of carrier concentration ratios between ZnO films grown with varying O_2 plasma times (solid dots) and thermal cycles (open dots)

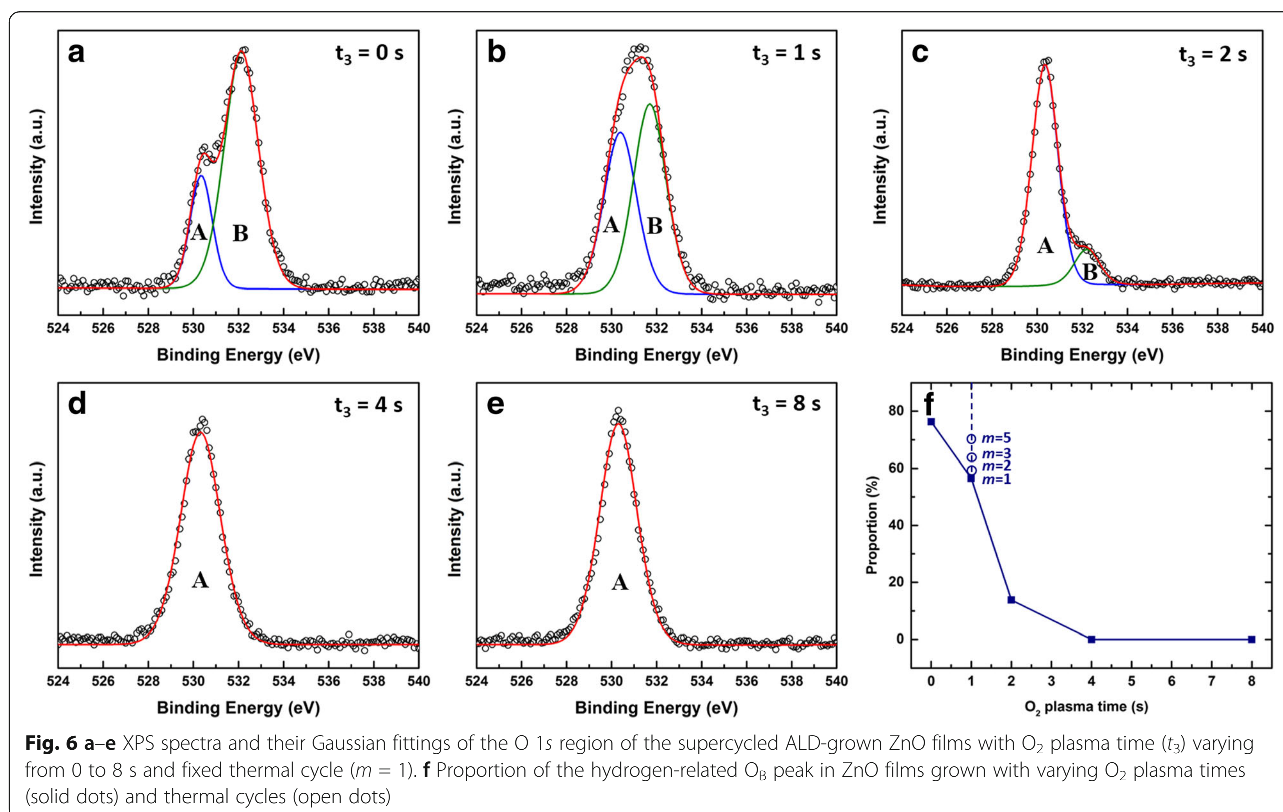

Fig. 6 **a**–**e** XPS spectra and their Gaussian fittings of the O 1*s* region of the supercycled ALD-grown ZnO films with O_2 plasma time (t_3) varying from 0 to 8 s and fixed thermal cycle (m = 1). **f** Proportion of the hydrogen-related O_B peak in ZnO films grown with varying O_2 plasma times (solid dots) and thermal cycles (open dots)

ions [33–35]. The assignments of the higher bonding energy component at ca. 532.2 (B) have been controversial over literatures [33–38]. However, it is widely reported that it is associated with the hydroxyl group (i.e., Zn–OH) [33, 37–39] in ZnO film. We therefore tentatively ascribe the O_B peak observed in Fig. 6 to the Zn–OH bonds. On the other hand, the oxygen vacancy-associated peak positioned at ca. 531.2 eV [35] is not observed in this work. ZnO film grown by the thermal ALD process (t_3 = 0 s) characterizes a dominant O_B peak in the XPS spectrum (Fig. 6a). This implies the existence of large amount of hydrogen-related impurities in this film. This high level of defects serves as a self-doping mechanism and leads to a high carrier concentration. The extra O_2 plasma step (t_3) diminishes the impurities, and the O_B peak intensity decreases with longer O_2 plasma time (Fig. 6f). Similar trend was also observed for ZnO films grown from varying thermal cycles in which more thermal cycles lead to the increase of O_B peak intensity as shown in Fig. 6f and Additional file 1: Figure S6.

The origin of the intrinsic *n*-type conductivity in ZnO films is still controversial. Although conventional wisdom has attributed this conductivity to native defect (i.e., oxygen vacancies and Zn interstitials) [18, 40–44], it has been challenged by recent first-principles calculations [45]. Oxygen vacancies are also unlikely to contribute to such a high concentration level as numerous studies suggest they are deep rather than shallow donors and have high formation energies in *n*-type ZnO (and are therefore unlike to form) [41–44]. Additionally, the oxygen vacancy-related O 1*s* peak is also not observed in our XPS data shown in Fig. 6. Although Zn interstitials are shallow donors, they have been suggested to have high formation energies and are faster diffusers and hence are unlikely to be stable [41]. The XPS spectra of the Zn $2p_{3/2}$ state of the supercycled ALD-grown ZnO films with various O_2 plasma times are shown Fig. 7. All spectra are characterized by a similar peak positioned at ca. 1021.5 eV which can be attributed to the Zn^{2+} bonding in ZnO [6, 34, 46]. However, the Zn interstitial component at a slightly higher binding energy [6, 47] is not observed in all spectra. This suggests that the influence of Zn interstitial on the ZnO film conductivity can also be ruled out in this work.

Recently, hydrogen-related impurities/defects are proposed to play a role in the *n*-type conductivity in ZnO [33, 48]. The evidence of the existence of hydrogen bonds in ZnO has been demonstrated by Janotti et al. [48], and it have been suggested that those bonds are able to incorporate in high concentrations and behave as shallow donors [49–51]. Indeed, hydrogen is present in our supercycled ALD process as both precursor and H_2O contain hydrogen and a Zn–OH bond is produced

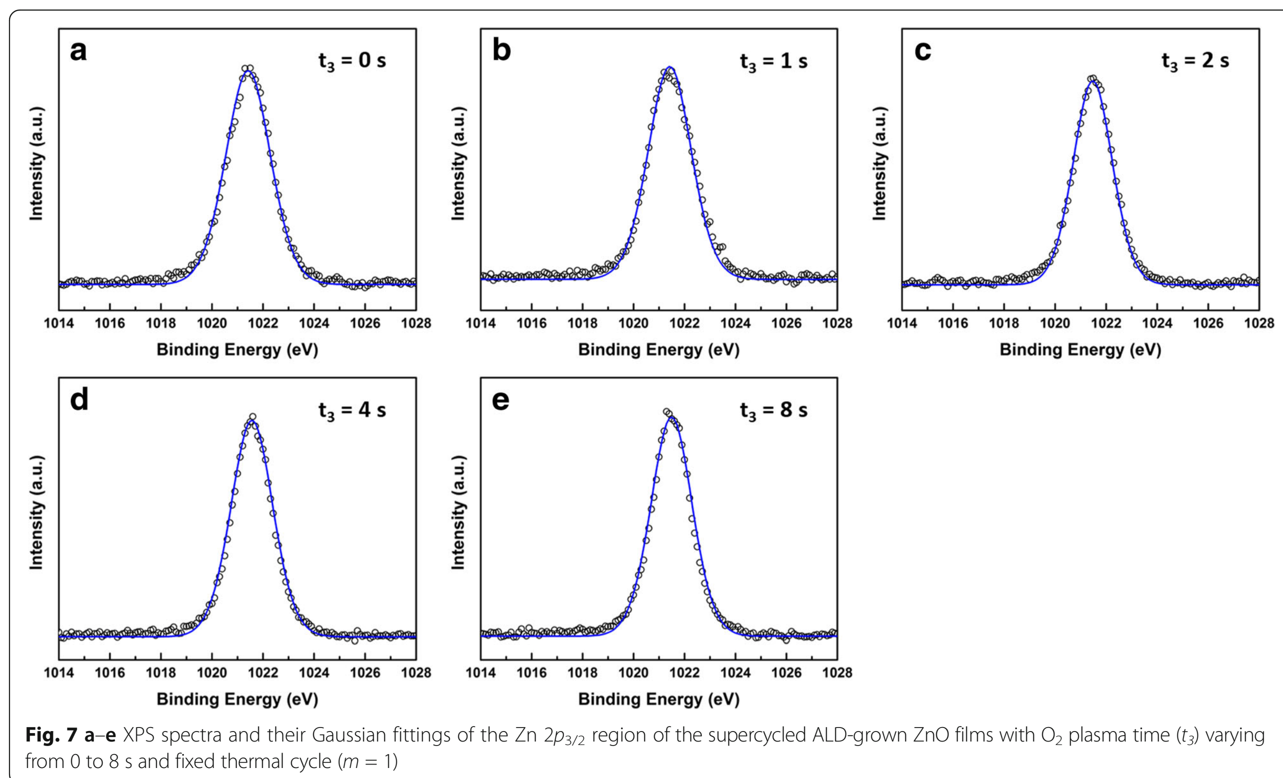

Fig. 7 a–e XPS spectra and their Gaussian fittings of the Zn $2p_{3/2}$ region of the supercycled ALD-grown ZnO films with O_2 plasma time (t_3) varying from 0 to 8 s and fixed thermal cycle (m = 1)

in every half cycle in the thermal ALD step. This is also supported by the observation of hydroxyl group-related O 1*s* peak in the XPS spectra (shown in Fig. 6). The ZnO film resistivity and carrier density are plotted against the proportion of this peak in Fig. 8. High proportion of these hydrogen impurities induce high carrier concentrations, leading to low resistivities. The subsequent O_2 plasma step within each supercycle reduces the carrier concentration by effectively removing the hydrogen bonds. This is accompanied by the reduction of carrier concentration as well as the increase of resistivity. Same behavior was also reported on both ALD and CVD processes [33, 52].

Conclusions

Deposition of undoped ZnO films with highly tunable electrical properties was reported here using a supercycled ALD process which combines a thermal ALD process and in situ O_2 plasma treatment. More than five orders of magnitude adjustment over the film resistivity and carrier concentration were achieved by tuning the O_2 plasma times. Finer tuning of the properties can also be realized by varying the number of thermal ALD cycles in a supercycle. The tuning of these electrical properties is believed to be associated with the change of hydrogen defect concentration in the film. This directly causes the shift of Fermi levels within the ZnO films as revealed by the Kelvin probe force microscopy. By adopting a simple electronic energy model, the carrier concentrations calculated from the Fermi level shifts demonstrate a good match with the Hall effect measurement results. This reliable and robust technique reported here clearly points towards the capability of using this method to produce ZnO films with controlled properties in different applications.

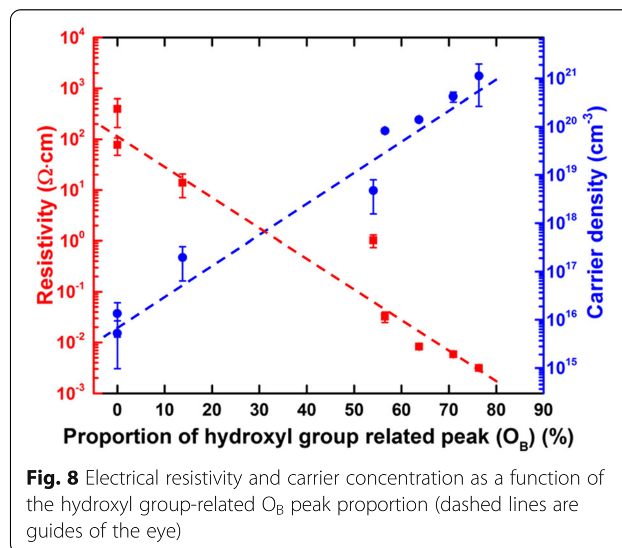

Fig. 8 Electrical resistivity and carrier concentration as a function of the hydroxyl group-related O_B peak proportion (dashed lines are guides of the eye)

Additional files

Additional file 1: Table S1. Process details for one growth supercycle in the supercycled ALD process used in this study. **Figure S1.** Diffraction intensity ratio of the ZnO (0 0 2) peak to (1 0 1) peak as a function of O_2 plasma times with fixed thermal cycle (m = 1). **Figure S2.** (a, d) The fitted refractive index n, (b, e) extinction coefficient k, and (c, f) plot of $(ahv)^2$ as a function of photo energy of ZnO films grown from different O_2 plasma times with fixed thermal cycle (m = 1) and different thermal cycles with fixed O_2 plasma time (t_3 = 1 s) by the supercycled ALD process. **Figure S3.** AFM images of the supercycled ALD-grown ZnO films with O_2 plasma times of (a) 0 s, (b) 1 s, (c) 2 s, (d) 4 s, and (e) 8 s and fixed thermal cycle (m = 1). **Figure S4.** Electronic energy levels of the tip sample system for three different cases. (a) Tip and sample are not electrically connected; (b) tip and sample are electrically connected with Fermi energy levels lined up; (c) an external bias equals to the contact potential difference V_{CPD} is applied to the tip. **Figure S5.** Two-dimensional contact potential difference V_{CPD} images of the surface potential measurements of the supercycled ALD-grown ZnO films with thermal cycles varying from (a) 2, (b) 3, and (c) 5 at fixed O_2 plasma time (t_3 = 1 s). **Figure S6.** XPS spectra and their Gaussian fittings of the O 1s region of the supercycled ALD-grown ZnO films with thermal cycles varying from (a) 2, (b) 3, and (c) 5 at fixed O_2 plasma time (t_3 = 1 s). (DOCX 1919 kb)

Abbreviations

ALD: Atomic layer deposition; DEZ: Diethylzinc; KPFM: Kelvin probe force microscopy; XPS: X-ray photoelectron spectroscopy; XRD: X-ray diffraction

Acknowledgements

We thank the Engineering and Physical Sciences Research Council (EPSRC) for a Doctoral Prize (R.H. EP/509015FP/1) and their support in XRD (EP/K00509X/1 and EP/K009877/1). All data can be found on dataset doi:10.5258/SOTON/D0248.

Authors' Contributions

RH, KS, and KSK conceived the idea and performed the ALD experiments; RH and SY undertook the material characterization: all authors contributed to the manuscript. All authors read and approved the final manuscript.

Competing Interests

The authors declare that they have no competing interests.

Publisher's Note

Springer Nature remains neutral with regard to jurisdictional claims in published maps and institutional affiliations.

Author details

[1]Nanoelectronics and Nanotechnology Group, Department of Electronics and Computer Science, University of Southampton, Southampton SO17 1BJ, UK. [2]Southampton Nanofabrication Centre, University of Southampton, Southampton SO17 1BJ, UK.

Received: 9 May 2017 Accepted: 8 September 2017
Published online: 19 September 2017

References

1. Janotti A, Van de Walle CG (2009) Fundamentals of zinc oxide as a semiconductor. Reports Prog Phys 72:126501. doi:10.1088/0034-4885/72/12/126501
2. Edwards PP, Porch A, Jones MO et al (2004) Basic materials physics of transparent conducting oxides. Dalt Trans:2995–3002. doi:10.1039/b408864f
3. Liu Y, Li Y, Zeng H (2013) ZnO-based transparent conductive thin films: doping, performance, and processing. J Nanomater 2013:196521. doi:10.1155/2013/196521
4. Ozgür M, Hofstetter D, Morkoç H (2010) ZnO devices and applications: a review of current status and future prospects. Proc IEEE 98:1255–1268. doi:10.1109/JPROC.2010.2044550
5. Fujita S (2015) Wide-bandgap semiconductor materials: for their full bloom. Jpn J Appl Phys 54:30101. doi:10.7567/JJAP.54.030101
6. Guziewicz E, Godlewski M, Wachnicki L et al (2012) ALD grown zinc oxide with controllable electrical properties. Semicond Sci Technol 27:74011. doi:10.1088/0268-1242/27/7/074011
7. Thomas G (1997) Materials science: invisible circuits. Nature 389:907–908. doi:10.1177/1754045313490905
8. Simanjuntak FM, Panda D, Wei K, Tseng T (2016) Status and prospects of ZnO-based resistive switching memory devices. Nanoscale Res Lett 11:368. doi:10.1186/s11671-016-1570-y
9. Cao X, Li X, Gao X et al (2011) All-ZnO-based transparent resistance random access memory device fully fabricated at room temperature. J Phys D Appl Phys 44:255104. doi:10.1088/0022-3727/44/25/255104
10. Mundle R, Carvajal C, Pradhan AK (2016) ZnO/Al:ZnO transparent resistive switching devices grown by atomic layer deposition for memristor applications. Langmuir 32:4983–4995. doi:10.1021/acs.langmuir.6b01014
11. Huang Q, Wang Y, Wang S et al (2012) Transparent conductive ZnO:B films deposited by magnetron sputtering. Thin Solid Films 520:5960–5964. doi:10.1016/j.tsf.2012.05.014
12. Sans JA, Sánchez-Royo JF, Segura A et al (2009) Chemical effects on the optical band-gap of heavily doped ZnO:M_{III} (M = Al, Ga, In): an investigation by means of photoelectron spectroscopy, optical measurements under pressure, and band structure calculations. Phys Rev B 79:195105. doi:10.1103/PhysRevB.79.195105
13. Bhachu DS, Sankar G, Parkin IP (2012) Aerosol assisted chemical vapor deposition of transparent conductive zinc oxide films. Chem Mater 24:4704–4710. doi:10.1021/cm302913b
14. Ellmer K, Bikowski A (2016) Intrinsic and extrinsic doping of ZnO and ZnO alloys. J Phys D Appl Phys 49:413002. doi:10.1088/0022-3727/49/41/413002
15. Johnson RW, Hultqvist A, Bent SF (2014) A brief review of atomic layer deposition: from fundamentals to applications. Mater Today 17:236–246. doi:10.1016/j.mattod.2014.04.026
16. Tynell T, Karppinen M (2014) Atomic layer deposition of ZnO: a review. Semicond Sci Technol 29:43001. doi:10.1088/0268-1242/29/4/043001
17. Kowalik IA, Guziewicz E, Kopalko K et al (2009) Structural and optical properties of low-temperature ZnO films grown by atomic layer deposition with diethylzinc and water precursors. J Cryst Growth 311:1096–1101. doi:10.1016/j.jcrysgro.2008.11.086
18. Godlewski M, Guziewicz E, Szade J et al (2008) Vertically stacked non-volatile memory devices—material considerations. Microelectron Eng 85:2434–2438. doi:10.1016/j.mee.2008.09.012
19. Sun K, Zeimpekis I, Hu C et al (2016) Low-cost top-down zinc oxide nanowire sensors through a highly transferable ion beam etching for healthcare applications. Microelectron Eng 153:96–100. doi:10.1016/j.mee.2016.02.016
20. Sultan SM, Sun K, Clark OD et al (2012) Electrical characteristics of top-down ZnO nanowire transistors using remote plasma ALD. IEEE Electron Device Lett 33:203–205. doi:10.1109/LED.2011.2174607
21. Huang R, Sun K, Kiang KS et al (2016) Forming-free resistive switching of tunable ZnO films grown by atomic layer deposition. Microelectron Eng 161:7–12. doi:10.1016/j.mee.2016.03.038
22. Nonnenmacher M, O'Boyle MP, Wickramasinghe HK (1991) Kelvin probe force microscopy. Appl Phys Lett 58:2921–2923. doi:10.1063/1.105227
23. Melitz W, Shen J, Kummel AC, Lee S (2011) Kelvin probe force microscopy and its application. Surf Sci Rep 66:1–27. doi:10.1016/j.surfrep.2010.10.001
24. Van Ben C, Cho HD, Kang TW, Yang W (2012) Doping transition of doped ZnO nanorods measured by Kelvin probe force microscopy. Thin Solid Films 520:4622–4625. doi:10.1016/j.tsf.2011.10.129
25. Su T, Zhang H-F (2012) Influence of oxygen partial pressure on the Fermi level of ZnO films investigated by Kelvin probe force microscopy. Chinese Phys Lett 29:127102. doi:10.1088/0256-307X/29/12/127102
26. Maragliano C, Lilliu S, Dahlem MS et al (2014) Quantifying charge carrier concentration in ZnO thin films by scanning Kelvin probe microscopy. Sci Rep 4:4203. doi:10.1038/srep04203
27. Jin M, Jo J, Neupane GP et al (2013) Tuning of undoped ZnO thin film via plasma enhanced atomic layer deposition and its application for an inverted polymer solar cell. AIP Adv 3:102114. doi:10.1063/1.4825230
28. Zhang JP, He G, Zhu LQ et al (2007) Effect of oxygen partial pressure on the structural and optical properties of ZnO film deposited by reactive sputtering. Appl Surf Sci 253:9414–9421. doi:10.1016/j.apsusc.2007.06.005
29. Patterson A (1939) The Scherrer formula for X-ray particle size determination. Phys Rev 56:978–982

30. Tan ST, Chen BJ, Sun XW et al (2005) Blueshift of optical band gap in ZnO thin films grown by metal-organic chemical-vapor deposition. J Appl Phys 98:13505. doi:10.1063/1.1940137
31. Agocs E, Fodor B, Pollakowski B et al (2014) Approaches to calculate the dielectric function of ZnO around the band gap. Thin Solid Films 571:684–688. doi:10.1016/j.tsf.2014.03.028
32. Cho EN, Park S, Yun I (2012) Spectroscopic ellipsometry modeling of ZnO thin films with various O_2 partial pressures. Curr Appl Phys 12:1606–1610. doi:10.1016/j.cap.2012.05.030
33. Thomas MA, Cui JB (2012) Highly tunable electrical properties in undoped ZnO grown by plasma enhanced thermal-atomic layer deposition. ACS Appl Mater Interfaces 4:3122–3128. doi:10.1021/am300458q
34. Ansari SA, Khan MM, Kalathil S et al (2013) Oxygen vacancy induced band gap narrowing of ZnO nanostructures by an electrochemically active biofilm. Nano 5:9238. doi:10.1039/c3nr02678g
35. Zhang X, Qin J, Xue Y et al (2014) Effect of aspect ratio and surface defects on the photocatalytic activity of ZnO nanorods. Sci Rep 4:4596. doi:10.1038/srep04596
36. Ahn CH, Kim JH, Cho HK (2012) Tunable electrical and optical properties in composition controlled Hf:ZnO thin films grown by atomic layer deposition. J Electrochem Soc 159:H384–H387. doi:10.1149/2.026204jes
37. Chen M, Wang X, Yu Y et al (2000) X-ray photoelectron spectroscopy and auger electron spectroscopy studies of Al-doped ZnO films. Appl Surf Sci 158:134–140. doi:10.1016/S0169-4332(99)00601-7
38. Hsu J-C, Lin Y-H, Wang PW, Chen Y-Y (2012) Spectroscopic ellipsometry studies on various zinc oxide films deposited by ion beam sputtering at room temperature. Appl Opt 51:1209. doi:10.1364/AO.51.001209
39. Park S-M, Ikegami T, Ebihara K (2006) Effects of substrate temperature on the properties of Ga-doped ZnO by pulsed laser deposition. Thin Solid Films 513:90–94. doi:10.1016/j.tsf.2006.01.051
40. Chang C-Y, Tsai F-Y (2011) Efficient and air-stable plastics-based polymer solar cells enabled by atomic layer deposition. J Mater Chem 21:5710. doi:10.1039/c0jm04066e
41. Janotti A, Van de Walle CG (2007) Native point defects in ZnO. Phys Rev B 76:165202. doi:10.1103/PhysRevB.76.165202
42. Look DC, Hemsky JW, Sizelove JR (1999) Residual native shallow donor in ZnO. Phys Rev Lett 82:2552–2555. doi:10.1103/PhysRevLett.82.2552
43. Zhang SB, Wei S-H, Zunger A (2001) Intrinsic n-type versus p-type doping asymmetry and the defect physics of ZnO. Phys Rev B 63:75205. doi:10.1103/PhysRevB.63.075205
44. Kohan A, Ceder G, Morgan D, Van de Walle C (2000) First-principles study of native point defects in ZnO. Phys Rev B 61:15019–15027
45. Janotti A, Van de Walle CG (2005) Oxygen vacancies in ZnO. Appl Phys Lett 87:122102. doi:10.1063/1.2053360
46. Lupan O, Pauporté T, Chow L et al (2010) Effects of annealing on properties of ZnO thin films prepared by electrochemical deposition in chloride medium. Appl Surf Sci 256:1895–1907. doi:10.1016/j.apsusc.2009.10.032
47. Kayaci F, Vempati S, Donmez I et al (2014) Role of zinc interstitials and oxygen vacancies of ZnO in photocatalysis: a bottom-up approach to control defect density. Nano 6:10224. doi:10.1039/C4NR01887G
48. Janotti A, Van de Walle CG (2007) Hydrogen multicentre bonds. Nat Mater 6:44–47. doi:10.1038/nmat1795
49. Van De Walle CG (2000) Hydrogen as a cause of doping in zinc oxide. Phys Rev Lett 85:1012–1015. doi:10.1103/PhysRevLett.85.1012
50. Wardle MG, Goss JP, Briddon PR (2005) Theory of Fe, Co, Ni, Cu, and their complexes with hydrogen in ZnO. Phys Rev B 72:155108. doi:10.1103/PhysRevB.72.155108
51. Lavrov E, Börrnert F, Weber J (2005) Photoconductivity and infrared absorption study of hydrogen-related shallow donors in ZnO. Phys Rev B 72:85212. doi:10.1103/PhysRevB.72.085212
52. Hlaing Oo WM, McCluskey MD, Huso J, Bergman L (2007) Infrared and Raman spectroscopy of ZnO nanoparticles annealed in hydrogen. J Appl Phys 102:43529. doi:10.1063/1.2773635

Submit your manuscript to a SpringerOpen journal and benefit from:

- ► Convenient online submission
- ► Rigorous peer review
- ► Open access: articles freely available online
- ► High visibility within the field
- ► Retaining the copyright to your article

Submit your next manuscript at ► springeropen.com